



HAL
open science

Dymeclin deficiency causes postnatal microcephaly, hypomyelination and reticulum-to-Golgi trafficking defects in mice and humans

Nina Dupuis, Assia Fafouri, Aurélien Bayot, Manoj Kumar, Tifenn Lecharpentier, Gareth Ball, David A. Edwards, Véronique Bernard, Pascal Dournaud, Séverine Drunat, et al.

► To cite this version:

Nina Dupuis, Assia Fafouri, Aurélien Bayot, Manoj Kumar, Tifenn Lecharpentier, et al.. Dymeclin deficiency causes postnatal microcephaly, hypomyelination and reticulum-to-Golgi trafficking defects in mice and humans. *Human Molecular Genetics*, 2015, 24 (10), pp.2771-2783. 10.1093/hmg/ddv038 . hal-02324809

HAL Id: hal-02324809

<https://hal.science/hal-02324809>

Submitted on 2 Jun 2020

HAL is a multi-disciplinary open access archive for the deposit and dissemination of scientific research documents, whether they are published or not. The documents may come from teaching and research institutions in France or abroad, or from public or private research centers.

L'archive ouverte pluridisciplinaire **HAL**, est destinée au dépôt et à la diffusion de documents scientifiques de niveau recherche, publiés ou non, émanant des établissements d'enseignement et de recherche français ou étrangers, des laboratoires publics ou privés.

1
2
3
4 **Dymeclin deficiency causes postnatal microcephaly, hypomyelination**
5 **and reticulum-to-Golgi trafficking defects in mice and humans**
6
7
8
9

10 Nina Dupuis^{1,2*}, Assia Fafouri^{1,2*}, Aurélien Bayot^{1,2}, Manoj Kumar^{1,2}, Tifenn Lecharpentier^{1,2},
11 Gareth Ball⁴, David Edwards⁴, Véronique Bernard^{5,6}, Pascal Dournaud^{1,2}, Séverine Drunat¹⁻³, Marie
12 Vermelle-Andrzejewski⁷, Catheline Vilain⁸, Marc Abramowicz⁸, Julie Désir^{8,9}, Jacky
13 Bonaventure^{10,12}, Nelly Gareil^{11, 12}, Gaëlle Boncompain^{11,12}, Zsolt Csaba^{1,2}, Franck Perez^{11,12},
14 Sandrine Passemard^{1-3**}, Pierre Gressens^{1,2,4**}, Vincent El Ghouzzi^{1,2}
15
16
17
18
19
20
21
22
23

- 24 1. Inserm, U1141, Paris, France
25 2. Univ Paris Diderot, Sorbonne Paris Cité, UMRS 1141, Paris, France
26 3. AP HP, Hôpital Robert Debré, Service de Génétique Clinique, Paris, France
27 4. Centre for the Developing Brain, Department of Division of Imaging Sciences and
28 Biomedical Engineering, King's College London, King's Health Partners, St. Thomas'
29 Hospital, London, United Kingdom
30 5. Inserm, U952, CNRS UMR7224, Paris, France
31 6. Université Pierre et Marie Curie, Paris, France
32 7. Hôpital Roger Salengro, Service de Neuropédiatrie, Lille, France
33 8. Medical Genetics Department, Hôpital Erasme, Université Libre de Bruxelles (ULB),
34 Brussels, Belgium
35 9. Institut de Pathologie et de Génétique, Gosselies, Belgium
36 10. CNRS UMR3347, Orsay, France
37 11. CNRS UMR144, Paris, France
38 12. Institut Curie, Centre de Recherche, Paris, France
39
40
41
42
43
44
45
46
47

48
49 *, ** Both authors equally contributed to this work
50
51

52 **Correspondence to:** Dr Vincent El Ghouzzi
53 Address: Inserm U1141, Hôpital Robert-Debré, 48 Boulevard Sérurier,
54 F-75019, Paris, France.
55 E-mail: vincent.elghouzzi@inserm.fr
56 Phone: +331 40031973, Fax: +331 40031995
57
58
59
60

1
2
3 **Running Title:** Dymeclin deficiency in the brain
4

5
6 **Number of characters in the running head:** 32
7

8
9 **Number of characters in the main title:** 128
10

11
12 **Number of words in the abstract:** 201
13

14
15
16 **Number of words in the manuscript (excluding abstract references and figure legends):** 4148
17

18
19 **Number of figures:** 10 (including 2 supplementary figures)
20

21
22 **Conflict of interest:** None
23
24
25
26
27
28
29
30
31
32
33
34
35
36
37
38
39
40
41
42
43
44
45
46
47
48
49
50
51
52
53
54
55
56
57
58
59
60

ABSTRACT

Dymeclin is a Golgi-associated protein whose deficiency causes Dyggve-Melchior-Clausen syndrome (DMC, MIM #223800), a rare recessively-inherited spondyloepimetaphyseal dysplasia consistently associated with postnatal microcephaly and intellectual disability. While the skeletal phenotype of DMC patients has been extensively described, very little is known about their cerebral anomalies, which result in brain growth defects and cognitive dysfunction. We used *Dymeclin*-deficient mice to determine the cause of microcephaly and to identify defective mechanisms at the cellular level. Brain weight and volume were reduced in all mutant mice from postnatal day 5 onward. Mutant mice displayed a narrowing of the frontal cortex, although cortical layers were normally organized. Interestingly, the corpus callosum was markedly thinner, a characteristic we also identified in DMC patients. Consistent with this, the myelin sheath was thinner, less compact and not properly rolled, while the number of mature oligodendrocytes and their ability to produce myelin basic protein were significantly decreased. Finally, cortical neurons from mutant mice and primary fibroblasts from DMC patients displayed substantially delayed endoplasmic reticulum to Golgi trafficking, that could be fully rescued upon Dymeclin re-expression. These findings indicate that Dymeclin is crucial for proper myelination and anterograde neuronal trafficking, two processes that are highly active during postnatal brain maturation.

Key words: Dymeclin, Golgi apparatus, Microcephaly, Myelin sheath, Trafficking

INTRODUCTION

Dyggve-Melchior-Clausen syndrome (DMC, MIM #223800) is a severe autosomal-recessive spondyloepimetaphyseal dysplasia associated with microcephaly and intellectual disability, caused by loss-of-function mutations in the *DYM* gene encoding DYMECLIN, a Golgi protein thought to be involved in intracellular trafficking (1-3). The skeletal manifestations of the disease include short-trunk dwarfism with specific radiological features, severe proximal limb shortening and facial dysmorphism (4). Microcephaly is also consistently observed in DMC along with mild-to-severe intellectual disability, frequently including poor or absent language acquisition (5-9). Interestingly, both skeletal growth defects and microcephaly develop during childhood and are therefore rarely diagnosed at birth. This suggests that the physiological mechanisms affected in DMC involve postnatal processes. Interestingly, Smith-McCort Dysplasia 1 (SMC1, MIM #607326), an allelic spondyloepimetaphyseal dysplasia with skeletal features identical to DMC but with normal intelligence and no microcephaly, also results from mutations in *DYM* (10, 11), whereas Smith-McCort Dysplasia 2 (SMC2, MIM #615222) is caused by homozygous mutations in *RAB33B*, another Golgi protein involved in trafficking (12, 13). Importantly, *DYM* mutations causing SMC1 consist of missense substitutions that do not lead to protein degradation but may instead result in some residual activity of the protein. In contrast, DMC is associated with truncating mutations predicted to induce a loss of *DYM* function (1). This suggests that the cerebral phenotype is associated with a complete deficiency of DYMECLIN and that its role in the brain could be different from that in the bone. Biochemical and live-imaging studies indicate that DYMECLIN is associated with Golgi membranes (1, 3) and is perpetually shuttled between the Golgi and cytosolic pools in a highly dynamic manner (1). Consistent with this, several Golgi vesicle proteins have been identified as potential DYMECLIN interactors (3, 14). These findings argue for a role of *DYM* in Golgi homeostasis and/or Golgi-associated vesicular trafficking. Mice deficient in Dymeclin develop progressive skeletal abnormalities reminiscent of human

1 DMC/SMC phenotypes (3). However, the brain phenotype of these mutant mice has never been
2
3 investigated.

4
5 In this study, we analyzed the cerebral phenotype of *Dym*-deficient mice as well as two DMC
6
7 patients to understand the role of Dymeclin in brain development. We found that *Dym*-deficient
8
9 mice developed microcephaly postnatally, with a narrowing of the frontal cortex, a thinner corpus
10
11 callosum associated with hypomyelinated axons and a reduced number of oligodendrocytes. This
12
13 was accompanied at the cellular level by an enlarged Golgi apparatus in both mature
14
15 oligodendrocytes and cortical neurons. While oligodendrocytes showed a reduced capacity to
16
17 produce the myelin basic protein (MBP), cortical neurons showed a strong impairment of
18
19 endoplasmic reticulum (ER)-to-Golgi transport, a function also altered in fibroblasts from DMC
20
21 patients. Furthermore, we found that in addition to postnatal microcephaly, the brains of the two
22
23 patients with DMC displayed a thinning of the corpus callosum, reinforcing the link between
24
25 altered Dymeclin function and brain development.
26
27
28
29
30
31
32
33
34
35
36
37
38
39
40
41
42
43
44
45
46
47
48
49
50
51
52
53
54
55
56
57
58
59
60

RESULTS

Dym^{-/-} mice develop postnatal microcephaly

In humans, most microcephalies are congenital, but some occur after birth and become more pronounced during childhood (15). To determine whether the *Dym* mutation causes microcephaly in mice, we used homozygous *Dym*-mutant mice lacking normal *Dym* transcript expression and previously shown to develop chondrodysplasia similar to that of DMC/SMC (3). We first macroscopically examined whole brains from young adult *Dym*^{-/-} and WT mice at P30. Most *Dym*^{-/-} brains appeared smaller in size. The length of the anteroposterior and dorsoventral axes was reduced and the frontal part of the cortex was narrowed (Fig. 1A). Brain weight was found to be systematically reduced in both males and females, with an average weight of 0.382g (\pm 0.005g) for *Dym*^{-/-} brains versus 0.432g (\pm 0.003g) for WT brains. The brain weight of heterozygous animals was similar to that of WT animals (Fig. 1B). To determine whether this weight reduction was already present at birth or appeared postnatally, we compared brain weight at birth (P0), P5 and P30. At P0, the difference in brain weight was hardly noticeable. In contrast, at P5, the brain weight of *Dym*^{-/-} animals was reduced by 10.2% in comparison with those of WT littermates (Fig. 1B). This difference remained stable up to adulthood, as the brain weight of *Dym*^{-/-} animals at P30 was lower by 11.0% compared with WT or heterozygous littermates (Fig. 1B). Again, no sex-related differences were noted (not shown). To measure the difference in brain volume, volumetric MRI was performed. Whole brain tissue volume, estimated from manual masking of the structural MRI, was reduced in *Dym*^{-/-} mice (mean volume in WT: 0.35 \pm 0.063 ml; in *Dym*^{-/-}: 0.29 \pm 0.022 ml). Deformation-based morphometry (DBM) revealed local volumetric reductions in the frontal cortex, white matter and inferior structures, including the brain stem (Fig. 1C). Together, these data indicate that *Dym*^{-/-} mice display a reduction in brain weight and volume and develop microcephaly during the postnatal period.

1
2
3 ***Dym*^{-/-} mice have a smaller frontal cortex and narrowed external capsule and corpus**
4 **callosum**
5
6

7
8 To determine which parts of the brain are affected in *Dym*^{-/-} mice, we analyzed coronal sections
9
10 counterstained with cresyl violet at P30. Five reference planes were chosen for comparisons
11
12 between *Dym*^{-/-} and WT brains (anterior (a) to posterior (e)), based on the Franklin & Paxinos
13
14 mouse brain atlas (Fig. 2A). Interestingly, the length of the anteroposterior axis was found to be
15
16 significantly reduced in *Dym*^{-/-} brains as compared to WT brains (by 9.73%, Fig. 2B). The
17
18 dorsoventral axis was also reduced in the anterior part of the brain (plane a, 4.8%, plane b, 4%). In
19
20 contrast, no difference in the mediolateral axis was noted between the two groups (not shown).
21
22 Given that reduced cerebral cortical development is the most common cause of inherited primary
23
24 microcephaly (16), we next examined the architecture of the cortex, its surface area and its
25
26 thickness in the five reference planes. The cortical surface area was reduced by 8% in *Dym*^{-/-}
27
28 brains, but this reduction was restricted to the most anterior part (Fig. 2C), consistent with a
29
30 narrowing of the frontal cortex. The six cortical layers appeared properly organized and cortical
31
32 thickness did not differ from controls (not shown), except in the most anterior part (Fig. 3A). This
33
34 reduction of the frontal cortical thickness was not due to a decreased cell density (Fig. 3C) but to a
35
36 significant shortening of the deeper layers (V-VI) (Fig. 3B). In addition, the area comprising the
37
38 corpus callosum and the external capsule was reduced in all planes, suggesting possible defects in
39
40 the white matter (Fig. 2D).
41
42
43
44
45
46
47

48 **Myelin is abnormal in *Dym*^{-/-} brains**
49

50 In keeping with the results above, we next examined the expression of MBP, one of the most
51
52 abundant components of the myelin membrane in the CNS and therefore a good marker for white
53
54 matter. Immunohistochemical labeling of P30 sections with an anti-MBP antibody confirmed the
55
56 reduction in the surface area of the corpus callosum in *Dym*^{-/-} brains (Fig. 3D and E), and
57
58 densitometry further revealed a reduction in MBP expression (Fig. 3E). Reduced protein levels
59
60

1 were confirmed by western blotting of whole brain extracts (Fig. 3F). Electron microscopic
2 analyses of the white matter revealed thin, poorly compacted and incorrectly rolled myelin sheaths
3 in *Dym*^{-/-} mutants (Fig. 4A). In contrast, the number of axons and their diameters were similar in
4 both groups (Fig. 4B). Measurement of the G-ratio (axon diameter/total fiber diameter) confirmed
5 the strong reduction of the myelin sheath thickness (Fig. 4B). Moreover, the density of
6 oligodendrocytes (the myelin-forming cells in the CNS), labeled with an antibody to Olig2
7 (expressed at all stages of oligodendrocytic maturation) was significantly decreased in the corpus
8 callosum of *Dym*^{-/-} animals at P30 as compared to their wild-type littermates (Fig. 4C and D
9 upper panels). A similar decrease in oligodendrocytic density was measured in sections labeled
10 with APC, a marker specific for mature oligodendrocytes (Fig. 4C and D lower panels). While no
11 cell death was detected in adults, at P5, cleaved-caspase 3 labeling revealed an increased amount
12 of apoptotic nuclei in the corpus callosum of *Dym*^{-/-} animals (Fig. 5D). TUNEL and Olig2 co-
13 labeling confirmed that these dying cells were oligodendrocytes (Fig. 5C and D). Together, these
14 data indicate that white matter volume is reduced in *Dym*^{-/-} brains due to a decrease in the number
15 of oligodendrocytes and axonal hypomyelination.

36 **The Golgi apparatus is markedly enlarged in *Dym*^{-/-} neurons and oligodendrocytes**

37 As also observed by Denais and colleagues (14), the Golgi apparatus was markedly disorganized
38 in primary fibroblasts from DMC patients (Supplementary Fig. 1A). In an effort to understand the
39 link between the defective white matter and cortical development on the one hand and Dymeclin
40 function on the other, we examined the structure and function of the Golgi apparatus in primary
41 neurons and oligodendrocytes from *Dym*^{-/-} mice. In primary cortical neuronal cultures from the
42 telencephalon from E14.5 mouse embryos, co-labeling for GM130, a marker of the cis-Golgi
43 apparatus, and NeuN, a neuronal marker, revealed a marked enlargement of Golgi stacks in *Dym*
44 ^{-/-} cells (Fig. 5A and B). In oligodendrocytes from glial-enriched primary cultures prepared from
45 mouse forebrains dissected at P0, the co-labeling of mature oligodendrocytes with GM130 and
46 APC also revealed an abnormally large Golgi apparatus in *Dym*^{-/-} cultures (Fig. 5A and B).

1 Confirming these results, the Golgi apparatus of mature neurons and oligodendrocytes was
2 markedly enlarged in cultures differentiated from *Dym*^{-/-} embryonic stem cells (Supplementary
3 Fig. 1B). Consistent with *in vivo* observations, co-labeling with the nuclear marker Olig2 and
4 MBP revealed that the number of oligodendrocytes able to express MBP was reduced significantly
5 in *Dym*^{-/-} cultures (Fig. 5C and D). Further, *Dym*^{-/-} oligodendrocytes expressing MBP appeared
6 poorly developed and less branched (Fig. 5C and D). Together, these results indicate that Golgi
7 structure is perturbed in *Dym*-deficient neurons and oligodendrocytes and could result in
8 maturation or trafficking defects.
9

20 Anterograde trafficking is impaired in *Dym*^{-/-} neurons and in human DMC fibroblasts

21 An extensive ER with dilated cisternae has been reported as a hallmark of *Dym* deficiency in
22 fibroblasts and chondrocytes from both DMC patients (4, 17, 18) and *Dym*^{-/-} mice (3). Since the
23 Golgi apparatus is affected in *Dym*-deficient neurons, we asked whether Dymeclin could be
24 involved in anterograde, i.e. ER-to-Golgi, trafficking. To examine trafficking between these two
25 compartments in cortical neurons, we analyzed the retention and release of a Golgi enzyme,
26 mannosidase II (ManII) using the Retention Using Selective Hooks (RUSH) system (19). In this
27 system, the ManII-SBP-GFP fusion protein is initially sequestered in the ER by the KDEL hook
28 until Biotin is added to the culture medium. At steady state, ManII-SBP-GFP was found in the ER
29 as expected in both WT and *Dym*^{-/-} neurons (Fig. 6). One hour after the addition of biotin, which
30 releases SBP from its local hook protein and triggers ManII translocation, we detected ManII-
31 SBP-GFP in the Golgi apparatus in half of the transfected neurons from WT cultures. Two hours
32 after biotin addition, ManII-SBP-GFP was fully translocated to the Golgi apparatus of almost all
33 WT neurons. In contrast, ManII-SBP-GFP was still detected in the ER compartment in the
34 majority of *Dym*^{-/-} neurons even two hours after biotin addition (Fig. 6). These data show that ER-
35 to-Golgi anterograde trafficking is impaired in *Dym*-deficient neurons. To check whether this
36 phenomenon could also occur in human DMC cells, we used the same RUSH assay in primary
37 fibroblasts from two patients with previously characterized *DYM* mutations (2, 4). Comparable
38
39
40
41
42
43
44
45
46
47
48
49
50
51
52
53
54
55
56
57
58
59
60

1 results were obtained with these DMC fibroblasts, although 40-50% of the transfected cells finally
2 displayed the localization of the reporter in the Golgi apparatus after 2 hours of biotin treatment
3 (Fig. 7). To confirm that the delay in anterograde trafficking was due to the deficiency of
4 Dymeclin, we repeated the RUSH assay in mouse neurons or human fibroblasts overexpressing
5 wild-type Dym-GFP, using a red fluorescent version (mCherry) of the Mannosidase II reporter.
6 Two hours after the addition of biotin, ManII-SBP-mCherry was consistently detected in the Golgi
7 apparatus of both *Dym*^{-/-} neurons (Supplementary Fig. 2A) and DMC fibroblasts (Supplementary
8 Fig. 2B) overexpressing Dym-GFP. These data confirm that *Dym* deficiency results in defective
9 anterograde trafficking and suggests that Dymeclin is required for efficient ER-to-Golgi cargo
10 translocation both in human and mouse cells.
11
12
13
14
15
16
17
18
19
20
21
22
23
24
25
26

Corpus callosum thickness is reduced in DMC patients

27 Despite the observation of microcephaly and intellectual deficits associated with DMC, white
28 matter defects have not so far been documented in DMC patients, most likely because of the rarity
29 of the syndrome and the scarcity of cerebral data available. Given our demonstration of the
30 involvement of Dymeclin in neuronal and oligodendrocytic Golgi function in mice, we next
31 examined the thickness of the corpus callosum in cerebral MRIs of two other unrelated DMC
32 patients with well-characterized *DYM* mutations. Strikingly, these patients not only exhibited
33 microcephaly with a postnatal onset, the thickness of their corpus callosum was markedly reduced
34 (Fig. 8), consistent with our findings in the brain of *Dym*^{-/-} mice as well as the observation that
35 Dymeclin deficiency impairs Golgi function, and possibly as a consequence, proper myelination.
36 These findings provide additional support to a role for Dymeclin-mediated intracellular transport
37 in normal brain development.
38
39
40
41
42
43
44
45
46
47
48
49
50
51
52
53
54
55
56
57
58
59
60

DISCUSSION

Postnatal microcephaly is a hallmark of DMC syndrome, which is caused by loss-of-function mutations in the human *DYM* gene (1). Our results show that *Dym*-deficient mice are a suitable model to study the cerebral phenotype observed in DMC patients, and confirms clinical observations that DYMECLIN deficiency in the human brain induces postnatal-onset microcephaly. In agreement with the progressive appearance of microcephaly that continues during childhood, we observed a marked reduction in the thickness of the corpus callosum in *Dym*^{-/-} mice, in association with myelination defects, a largely postnatal process (20, 21). Interestingly, our study also reveals a marked thinning of the corpus callosum in two unrelated DMC patients, confirming our findings in mutant mice and suggesting that white matter defects are central to the pathophysiology of DMC syndrome. As the principal commissure interconnecting the two cerebral hemispheres, the corpus callosum contains more than 200 million axons, and volumetric alterations to this structure likely reflect more general white matter volume defects. Consistent with this hypothesis, the brain stem volume was also found to be reduced in *Dym*^{-/-} mice, and the medulla oblongata appeared distinctly narrower than normal in the brain MRI of Patient 2. Our data suggest that volumetric MRI to quantify white matter volume and density should be systematically performed in children with DMC to better characterize these newly identified structural anomalies, which might represent an important feature of the DMC brain phenotype. These findings also provide a relevant explanation for the low IQ and specific language difficulties frequently described in DMC patients, especially as previous studies have evidenced a substantial correlation between general intelligence and white matter volume (22, 23).

What is the mechanism underlying this postnatal development of white matter defects and microcephaly? Our data show that Dymeclin deficiency results in thinner, less compact and improperly rolled myelin membranes. In the CNS, myelination is carried out by oligodendrocytes, which enwrap axons to form the myelin sheath (24). Given that fewer oligodendrocytes were

1 found in *Dym*^{-/-} brains and that the remaining mature oligodendrocytes displayed an abnormal
2
3 Golgi structure along with a decreased ability to produce MBP, it is likely that Dymeclin is
4
5 required for full oligodendrocyte maturation. Oligodendrocytes send out plasma membrane
6
7 extensions that become more and more branched as the cell differentiates, allowing a single
8
9 mature oligodendrocyte to ensheath several axons. Although MBP proteins are synthesized
10
11 locally in these plasma membrane extensions following the specific transport of MBP mRNAs
12
13 (25), the sorting and transport of other myelin components and lipids requires intensive
14
15 trafficking, in which the Golgi apparatus actively participates and which could be impaired by
16
17 Dymeclin deficiency (26). In line with these observations, the Golgi apparatus displayed abnormal
18
19 morphology in *Dym*-deficient mouse neurons and in fibroblasts from DMC patients. In addition,
20
21 we observed slowed ER-to-Golgi trafficking in both cell types that could be completely rescued
22
23 upon *Dym*-GFP expression. This observation is in agreement with previous findings showing the
24
25 delayed relocation of GM130 to the Golgi in *Dym*^{-/-} mouse fibroblasts recovering from Brefeldin-
26
27 A treatment, which causes the reversible redistribution of Golgi membranes to the ER (3).
28
29 Moreover, DMC patient fibroblasts expressing naturally-secreted Gaussia luciferase (Gluc), used
30
31 to assess the efficiency of the secretory pathway (27), displayed reduced secretion capacities,
32
33 again implicating Dymeclin in anterograde trafficking (data not shown). These results potentially
34
35 uncover a novel link between the localization of Dymeclin in the Golgi apparatus, and the
36
37 appearance of structural brain defects including microcephaly.
38
39
40
41
42
43
44

45 In recent years, several Golgi-resident proteins have been implicated in genetic disorders that
46
47 involve postnatal-onset microcephaly, including RAB18, RAB1GAP and RAB2GAP in Warburg
48
49 Micro syndrome (28, 29), VPS53 in progressive cerebello-cerebral atrophy type 2 (30), and
50
51 TRAPPC9 in some idiopathic intellectual disability (31-33). Very interestingly, all these proteins
52
53 are directly involved in the activation/inactivation cycle of the Rab-GTPases (34), and play a role
54
55 in the regulation of Golgi vesicle trafficking. Moreover, their loss-of-function has been directly
56
57 associated with clinical features that include corpus callosum hypoplasia. Hence, our study, in
58
59
60

1 conjunction with the probable link between Dymeclin and RAB33 (12, 13), (i) indicates that
2
3 Dymeclin is involved in the regulation of Golgi vesicle trafficking in several cell types, including
4
5 oligodendrocytes and neurons and (ii) reinforces the hypothesis that the secretory functions of the
6
7 Golgi apparatus play a central role in the proper development and maturation of both the white
8
9 matter and cortex in humans and mice.
10

11
12
13
14 In conclusion, our data indicate that Dymeclin deficiency results in postnatal microcephaly
15
16 through a mechanism involving defective myelination and impaired Golgi trafficking in neural
17
18 cells. Further work is needed to explore the consequences of defective ER-to-Golgi anterograde
19
20 transport on myelination and axonal transport, and to understand the precise role of Dymeclin in
21
22 this process, and more widely the role of the secretory traffic in microcephaly.
23
24
25
26
27
28
29
30
31
32
33
34
35
36
37
38
39
40
41
42
43
44
45
46
47
48
49
50
51
52
53
54
55
56
57
58
59
60

MATERIALS AND METHODS

Immunohistochemistry and immunocytochemistry

Mice were sacrificed and the whole brain was dissected out from the level of the foramen magnum to the most rostral part including olfactory bulbs, immediately weighed, fixed in formalin and embedded in paraffin. Coronal sections 16 μ m-thick were mounted on gelatin-coated slides, stained with cresyl violet or immunolabeled with anti-MBP (1:100, MAB382, Millipore), anti-Olig2 (1:200, 18953, IBL), anti-APC (1:2000, OP80, Calbiochem), anti-Cux1 (1:200, sc-13024, Santa Cruz) or anti-Ctip2 (1:500, ab18465, Abcam) antibodies. Immunocytochemistry was performed as described (35) using anti-NeuN (1:500, MAB377, Millipore), anti-GM130 (1:200, 610822, BD), anti-Calnexin (1:2000, C4731, Sigma), anti-APC (1:2000, OP80, Calbiochem), anti-Giantin (1:2000, ab24586, Abcam), anti-MBP (1:500, MAB382, Millipore) and anti-MAP2 (1:200, ab11268, Abcam).

Histomorphometric analyses

Brains Coronal sections from P30 mice were stained with cresyl violet and imaged using a Zeiss SteREO Discovery.V12 microscope. Five anteroposterior levels (a-e) were selected based on relevant anatomical landmarks of wild-type mice (36) (from the interaural line/bregma respectively (in mm): 5.22/1.42 (a), 4.90/1.10 (b), 4.06/0.26 (c), 2.46/-1.34 (d), 1.50/-2.30 (e)). For each level, we measured (i) the dorsoventral and mediolateral axes, (ii) the surface area of the entire cortex, (iii) the surface area of the white matter comprising the corpus callosum and/or the external capsule, the boundary of the two structures being defined by the position of the cingulum, and (iv) the thickness of the motor and somatosensory cortex. The length of the anteroposterior axis was deduced from the number of sections generated between a and e. Measurements were done using Image-J software and quantitative data expressed as means \pm SEM.

Human and mouse MRI analyses

Human cerebral MRI was performed as described (37). For mouse MRI, brains (WT = 5, *Dym*^{-/-} = 5) were imaged on a 9.4T Varian scanner, using a 3D spoiled gradient echo sequence with a 100G/cm gradient-coil and 33mm Rapid RF quadrature volume-coil; TR 150ms, TE 4.6ms and flip angle 35°. For deformation-based morphometry (DBM), a single control mouse was chosen for reference images. All other images were aligned to this reference using affine followed by nonlinear registration implemented with the IRTK package (38, 39). A reference image was created by taking the intensity-average of the aligned images, and 3 further iterations of registration were performed, using an updated intensity average as the reference image. A measure of local volume change induced by the transformation between each image and the final reference image was obtained from the determinant of the Jacobian operator applied to the transformation. A voxelwise statistical comparison of volume relative to the reference image, represented by the Jacobian determinant, was performed with Randomise, implemented in FSL, v4.1 (40).

Primary cultures and transfection

Primary cortical neurons were extracted from the forebrain of E14.5 embryos using 0.25% trypsin dissociation (Invitrogen), 0.6mg/ml DNase I digestion (Sigma) and manual dissociation in Minimum Essential Medium (Sigma) supplemented with 10% horse serum, antibiotics, 2mM glutamine (Invitrogen), 7.5% sodium bicarbonate (Invitrogen) and 0.6% glucose (Sigma). Cells were maintained in Neurobasal medium (Invitrogen) supplemented with B21 (Miltenyi Biotech) and 5mM glutamine at 37°C in a humidified 5% CO₂ incubator. Primary oligodendrocytes were prepared from neonatal mouse brains and cells were maintained at 37°C in a humidified 5% CO₂ incubator for 7 days in proliferation medium (MEM (Invitrogen) supplemented with 10% Fetal Bovine Serum (Invitrogen), 1% glutamax and 0.5% glucose) and for 10 additional days in differentiation medium (DMEM-F12 (Invitrogen) supplemented with 1% N2 (Invitrogen),

1 40ng/ml T3 (Sigma)). Media were changed every alternate day. Neuronal transfection was adapted
2
3 from (41): At DIV5, half the medium (hM) was removed and kept at 37°C while neurons were
4
5 exposed to a calcium-phosphate/DNA complex for 60 min. Fresh medium pre-warmed in a 10%
6
7 CO₂ atmosphere for 4 hours was added to the culture to reduce calcium-phosphate-complex
8
9 toxicity. Neurons were rinsed with fresh medium and hM replaced. Human dermal fibroblasts
10
11 from DMC patients and unaffected age-matched individuals were derived from skin biopsies and
12
13 grown in MEM (Invitrogen) supplemented with 10% Fetal Bovine Serum (Invitrogen), 1%
14
15 glutamax, antibiotics and 0.5% glucose). For transfection, fibroblasts were electroporated using
16
17 the Neon transfection system (Invitrogen) and plated on coverslips for 24 h.
18
19
20
21
22

23 **Electron microscopy**

24
25 Mice were perfused transaortically with 20 ml saline followed by 100 ml of 2% paraformaldehyde
26
27 with 2% glutaraldehyde at 4°C. Brains were post-fixed in 2% paraformaldehyde at 4°C. Sagittal
28
29 sections 70 µm-thick were postfixed in 1% glutaraldehyde for 10 min, treated with 1% osmium
30
31 tetroxide for 10 min and dehydrated in an ascending series of ethanol solutions. Sections were
32
33 treated with propylene oxide, equilibrated in Durcupan ACM (Fluka), flat-embedded on glass
34
35 slides and cured at 60 °C for 48 h. Blocks of the trunk of the corpus callosum close to the midline
36
37 were cut out from the sections and glued to blank cylinders of resin. Ultrathin sections were cut on
38
39 a Reichert Ultracut S microtome, collected on pioloform-coated single-slot grids, stained with lead
40
41 citrate and analyzed using a Philips CM120 electron microscope equipped with Morada Imaging
42
43 System (Olympus).
44
45
46
47
48
49

50 **Western blot analysis**

51
52 Brains were dissected out from P30 mice (WT = 10, *Dym*^{-/-} = 10), crushed in lysis buffer
53
54 supplemented with protease inhibitors and centrifuged. Lysates were heat-denatured, separated by
55
56 SDS-PAGE and transferred to PVDF membranes. Membranes were probed with anti-MBP
57
58
59
60

1 (1:2000, MAB382, Millipore) or anti-actin antibodies (1:10000, MAB1501, Millipore). Signal
2
3 was detected by chemiluminescence and quantified using Image-J.
4
5
6
7

8 **Analysis of trafficking kinetics of the mannosidase II-SBP-EGFP cargo**

9
10 Trafficking kinetics between the ER and the Golgi were evaluated using the RUSH system (19).
11 Mouse primary cortical neurons or human fibroblasts transiently expressing KDEL-streptavidin as
12 a hook and the Golgi enzyme mannosidase II (ManII)-SBP-EGFP (or -mCherry) as a reporter
13 were imaged either before or 60 min and 120 min after biotin addition (40 μ M). Ten fields were
14 counted (40-100 transfected cells per condition) and each fluorescent cell classified according to
15 the location of the reporter in the ER, ER/Golgi or Golgi. Experiments were repeated three times,
16 independently.
17
18
19
20
21
22
23
24
25
26
27

28 **Animals and ethics statement**

29
30 *Dymeclin* mice were provided by Dr H.E. Ruley (Nashville, TN). Experimental mice were
31 obtained by mating heterozygous animals, except for primary cultures for which embryos were
32 generated from wild-type or *Dym*^{-/-} breeders. Genomic DNA from tails was used for genotyping.
33 Mice were housed with a 12h light/dark cycle with free access to food and water. The
34 experimental protocol (2010-13/676-0017) was approved by the National Debré-Bichat Ethics
35 Committee and applied in agreement with French laws on animal protection.
36
37
38
39
40
41
42
43
44

45 **Patients and ethics approval**

46 Experiments presented in the present study were approved by the Inserm Institutional Review
47 Board, and the human primary fibroblasts were derived from skin biopsies following written
48 informed consent from the patients or their parents.
49
50
51
52
53
54
55
56
57
58
59
60

ACKNOWLEDGMENTS

We are grateful to Prof. H. Earl Ruley and Dr Anna B. Osipovich, Vanderbilt University, Nashville, Texas for providing the Dym strain, to Prof. Vincent Lelièvre, Institut des Neurosciences Cellulaires et Intégratives de Strasbourg, France for assistance with histomorphometric analyses and fruitful discussions, to Dr S Rasika for relevant comments and language editing during the preparation of this manuscript and to Cécile Martel for invaluable support. This study was supported by the Institut National pour la Santé et la Recherche Médicale (Inserm), the Centre National de la Recherche Scientifique (CNRS), the Université Paris 7, and grants from the French National Research Agency (project ANR-09-GENO-007) and the Roger de Spoelberch Foundation. ND was funded by the Inserm Transfer program, MK was funded by the Inserm and ANR contract N°ANR-09-GENO-007 to VEG.

REFERENCES

- 1 Dimitrov, A., Paupe, V., Gueudry, C., Sibarita, J.B., Raposo, G., Vielemeyer, O., Gilbert, T.,
2
3
4
5
6 Csaba, Z., Attie-Bitach, T., Cormier-Daire, V. *et al.* (2009) The gene responsible for
7
8 Dyggve-Melchior-Clausen syndrome encodes a novel peripheral membrane protein
9
10 dynamically associated with the Golgi apparatus. *Hum Mol Genet*, **18**, 440-453.
11
12
- 13
14
15 2 El Ghouzzi, V., Dagoneau, N., Kinning, E., Thauvin-Robinet, C., Chemaitilly, W., Prost-
16
17 Squarcioni, C., Al-Gazali, L.I., Verloes, A., Le Merrer, M., Munnich, A. *et al.* (2003)
18
19 Mutations in a novel gene Dymeclin (FLJ20071) are responsible for Dyggve-Melchior-
20
21 Clausen syndrome. *Hum Mol Genet*, **12**, 357-364.
22
23
- 24
25 3 Osipovich, A.B., Jennings, J.L., Lin, Q., Link, A.J. and Ruley, H.E. (2008) Dyggve-Melchior-
26
27 Clausen syndrome: chondrodysplasia resulting from defects in intracellular vesicle traffic.
28
29 *Proc Natl Acad Sci U S A*, **105**, 16171-16176.
30
31
- 32
33 4 Paupe, V., Gilbert, T., Le Merrer, M., Munnich, A., Cormier-Daire, V. and El Ghouzzi, V.
34
35 (2004) Recent advances in Dyggve-Melchior-Clausen syndrome. *Mol Genet Metab*, **83**,
36
37 51-59.
38
39
- 40
41 5 Girisha, K.M., Cormier-Daire, V., Heuertz, S., Phadke, R.V. and Phadke, S.R. (2008) Novel
42
43 mutation and atlantoaxial dislocation in two siblings from India with Dyggve-Melchior-
44
45 Clausen syndrome. *Eur J Med Genet*, **51**, 251-256.
46
47
- 48
49 6 Khalifa, O., Imtiaz, F., Al-Sakati, N., Al-Manea, K., Verloes, A. and Al-Owain, M. (2011)
50
51 Dyggve-Melchior-Clausen syndrome: novel splice mutation with atlanto-axial subluxation.
52
53 *European journal of pediatrics*, **170**, 121-126.
54
55
- 56
57 7 Martinez-Frias, M.L., Cormier-Daire, V., Cohn, D.H., Mendioroz, J., Bermejo, E. and
58
59 Mansilla, E. (2007) [Dyggve-Melchior-Clausen syndrome: presentation of a case with a
60
mutation of possible Spanish origin]. *Medicina clinica*, **128**, 137-140.
- 8 Neumann, L.M., El Ghouzzi, V., Paupe, V., Weber, H.P., Fastnacht, E., Leenen, A., Lyding, S.,
Klusmann, A., Mayatepek, E., Pelz, J. *et al.* (2006) Dyggve-Melchior-Clausen syndrome

- 1 and Smith-McCort dysplasia: clinical and molecular findings in three families supporting
2 genetic heterogeneity in Smith-McCort dysplasia. *Am J Med Genet A*, **140**, 421-426.
- 3
4
5
6 9 Pogue, R., Ehtesham, N., Repetto, G.M., Carrero-Valenzuela, R., de Casella, C.B., de Pons,
7 S.P., Martinez-Frias, M.L., Heuertz, S., Cormier-Daire, V. and Cohn, D.H. (2005)
8 Probable identity-by-descent for a mutation in the Dyggve-Melchior-Clausen/Smith-
9 McCort dysplasia (Dymeclin) gene among patients from Guam, Chile, Argentina, and
10 Spain. *Am J Med Genet A*, **138**, 75-78.
- 11
12
13
14
15
16
17 10 Cohn, D.H., Ehtesham, N., Krakow, D., Unger, S., Shanske, A., Reinker, K., Powell, B.R. and
18 Rimoin, D.L. (2003) Mental retardation and abnormal skeletal development (Dyggve-
19 Melchior-Clausen dysplasia) due to mutations in a novel, evolutionarily conserved gene.
20
21
22
23
24
25
26 11 Santos, H.G., Fernandes, H.C., Nunes, J.L. and Almeida, M.R. (2009) Portuguese case of
27 Smith-McCort syndrome caused by a new mutation in the Dymeclin (FLJ20071) gene.
28
29
30
31
32
33
34 12 Alshammari, M.J., Al-Otaibi, L. and Alkuraya, F.S. (2012) Mutation in RAB33B, which
35 encodes a regulator of retrograde Golgi transport, defines a second Dyggve-Melchior-
36 Clausen locus. *J Med Genet*, **49**, 455-461.
- 37
38
39 13 Dupuis, N., Lebon, S., Kumar, M., Drunat, S., Graul-Neumann, L.M., Gressens, P. and El
40 Ghouzzi, V. (2013) A Novel RAB33B Mutation in Smith-McCort Dysplasia. *Hum Mutat*,
41
42
43
44
45
46 14 Denais, C., Dent, C.L., Southgate, L., Hoyle, J., Dafou, D., Trembath, R.C. and Machado, R.D.
47 (2011) Dymeclin, the gene underlying Dyggve-Melchior-Clausen syndrome, encodes a
48 protein integral to extracellular matrix and golgi organization and is associated with protein
49 secretion pathways critical in bone development. *Hum Mutat*, **32**, 231-239.
- 50
51
52
53
54 15 Rosman, N.P., Tarquinio, D.C., Datsaris, M., Hou, W., Mannheim, G.B., Emigh, C.E. and
55 Rivkin, M.J. (2011) Postnatal-onset microcephaly: pathogenesis, patterns of growth, and
56 prediction of outcome. *Pediatrics*, **127**, 665-671.
- 57
58
59
60

- 1
2
3
4
5
6
7
8
9
10
11
12
13
14
15
16
17
18
19
20
21
22
23
24
25
26
27
28
29
30
31
32
33
34
35
36
37
38
39
40
41
42
43
44
45
46
47
48
49
50
51
52
53
54
55
56
57
58
59
60
- 16 Kaindl, A.M., Passemard, S., Kumar, P., Kraemer, N., Issa, L., Zwirner, A., Gerard, B., Verloes, A., Mani, S. and Gressens, P. (2010) Many roads lead to primary autosomal recessive microcephaly. *Prog Neurobiol*, **90**, 363-383.
- 17 Engfeldt, B., Bui, T.H., Eklof, O., Hjerpe, A., Reinholt, F.P., Ritzen, E.M. and Wikstrom, B. (1983) Dyggve-Melchior-Clausen dysplasia. Morphological and biochemical findings in cartilage growth zones. *Acta paediatrica Scandinavica*, **72**, 269-274.
- 18 Nakamura, K., Kurokawa, T., Nagano, A., Nakamura, S., Taniguchi, K. and Hamazaki, M. (1997) Dyggve-Melchior-Clausen syndrome without mental retardation (Smith-McCort dysplasia): morphological findings in the growth plate of the iliac crest. *Am J Med Genet*, **72**, 11-17.
- 19 Boncompain, G., Divoux, S., Gareil, N., de Forges, H., Lescure, A., Latreche, L., Mercanti, V., Jollivet, F., Raposo, G. and Perez, F. (2012) Synchronization of secretory protein traffic in populations of cells. *Nature methods*, **9**, 493-498.
- 20 Bartzokis, G. (2004) Age-related myelin breakdown: a developmental model of cognitive decline and Alzheimer's disease. *Neurobiology of aging*, **25**, 5-18; author reply 49-62.
- 21 Sturrock, R.R. (1980) Myelination of the mouse corpus callosum. *Neuropathology and applied neurobiology*, **6**, 415-420.
- 22 Haier, R.J., Jung, R.E., Yeo, R.A., Head, K. and Alkire, M.T. (2004) Structural brain variation and general intelligence. *NeuroImage*, **23**, 425-433.
- 23 Posthuma, D., De Geus, E.J., Baare, W.F., Hulshoff Pol, H.E., Kahn, R.S. and Boomsma, D.I. (2002) The association between brain volume and intelligence is of genetic origin. *Nat Neurosci*, **5**, 83-84.
- 24 Baumann, N. and Pham-Dinh, D. (2001) Biology of oligodendrocyte and myelin in the mammalian central nervous system. *Physiological reviews*, **81**, 871-927.
- 25 Muller, C., Bauer, N.M., Schafer, I. and White, R. (2013) Making myelin basic protein -from mRNA transport to localized translation. *Frontiers in cellular neuroscience*, **7**, 169.

- 1 26 Kramer, E.M., Schardt, A. and Nave, K.A. (2001) Membrane traffic in myelinating
2 oligodendrocytes. *Microscopy research and technique*, **52**, 656-671.
- 3
4
5 27 Badr, C.E., Hewett, J.W., Breakefield, X.O. and Tannous, B.A. (2007) A highly sensitive assay
6 for monitoring the secretory pathway and ER stress. *PLoS One*, **2**, e571.
- 7
8
9 28 Bem, D., Yoshimura, S., Nunes-Bastos, R., Bond, F.C., Kurian, M.A., Rahman, F., Handley,
10 M.T., Hadzhiev, Y., Masood, I., Straatman-Iwanowska, A.A. *et al.* (2011) Loss-of-
11 function mutations in RAB18 cause Warburg micro syndrome. *Am J Hum Genet*, **88**, 499-
12 507.
- 13
14
15 29 Liegel, R.P., Handley, M.T., Ronchetti, A., Brown, S., Langemeyer, L., Linford, A., Chang, B.,
16 Morris-Rosendahl, D.J., Carpanini, S., Posmyk, R. *et al.* (2013) Loss-of-function mutations
17 in TBC1D20 cause cataracts and male infertility in blind sterile mice and Warburg micro
18 syndrome in humans. *Am J Hum Genet*, **93**, 1001-1014.
- 19
20
21 30 Feinstein, M., Flusser, H., Lerman-Sagie, T., Ben-Zeev, B., Lev, D., Agamy, O., Cohen, I.,
22 Kadir, R., Sivan, S., Leshinsky-Silver, E. *et al.* (2014) VPS53 mutations cause progressive
23 cerebello-cerebral atrophy type 2 (PCCA2). *J Med Genet*, **51**, 303-308.
- 24
25
26 31 Mir, A., Kaufman, L., Noor, A., Motazacker, M.M., Jamil, T., Azam, M., Kahrizi, K., Rafiq,
27 M.A., Weksberg, R., Nasr, T. *et al.* (2009) Identification of mutations in TRAPPC9, which
28 encodes the NIK- and IKK-beta-binding protein, in nonsyndromic autosomal-recessive
29 mental retardation. *Am J Hum Genet*, **85**, 909-915.
- 30
31
32 32 Mochida, G.H., Mahajnah, M., Hill, A.D., Basel-Vanagaite, L., Gleason, D., Hill, R.S., Bodell,
33 A., Crosier, M., Straussberg, R. and Walsh, C.A. (2009) A truncating mutation of
34 TRAPPC9 is associated with autosomal-recessive intellectual disability and postnatal
35 microcephaly. *Am J Hum Genet*, **85**, 897-902.
- 36
37
38 33 Philippe, O., Rio, M., Carioux, A., Plaza, J.M., Guigue, P., Molinari, F., Boddaert, N., Bole-
39 Feysot, C., Nitschke, P., Smahi, A. *et al.* (2009) Combination of linkage mapping and
40 microarray-expression analysis identifies NF-kappaB signaling defect as a cause of
41 autosomal-recessive mental retardation. *Am J Hum Genet*, **85**, 903-908.
- 42
43
44
45
46
47
48
49
50
51
52
53
54
55
56
57
58
59
60

- 1
2
3
4
5
6
7
8
9
10
11
12
13
14
15
16
17
18
19
20
21
22
23
24
25
26
27
28
29
30
31
32
33
34
35
36
37
38
39
40
41
42
43
44
45
46
47
48
49
50
51
52
53
54
55
56
57
58
59
60
- 34 Hutagalung, A.H. and Novick, P.J. (2011) Role of Rab GTPases in membrane traffic and cell physiology. *Physiological reviews*, **91**, 119-149.
- 35 Srivastava, R., Kumar, M., Peineau, S., Csaba, Z., Mani, S., Gressens, P. and El Ghouzzi, V. (2013) Conditional induction of Math1 specifies embryonic stem cells to cerebellar granule neuron lineage and promotes differentiation into mature granule neurons. *Stem Cells*, **31**, 652-665.
- 36 KBJ, P.G.a.F. (2007), in press.
- 37 Falip, C., Blanc, N., Maes, E., Zaccaria, I., Oury, J.F., Sebag, G. and Garel, C. (2007) Postnatal clinical and imaging follow-up of infants with prenatal isolated mild ventriculomegaly: a series of 101 cases. *Pediatric radiology*, **37**, 981-989.
- 38 Rueckert, D., Frangi, A.F. and Schnabel, J.A. (2003) Automatic construction of 3-D statistical deformation models of the brain using nonrigid registration. *IEEE transactions on medical imaging*, **22**, 1014-1025.
- 39 Rueckert, D., Sonoda, L.I., Hayes, C., Hill, D.L., Leach, M.O. and Hawkes, D.J. (1999) Nonrigid registration using free-form deformations: application to breast MR images. *IEEE transactions on medical imaging*, **18**, 712-721.
- 40 Smith, S.M., Jenkinson, M., Woolrich, M.W., Beckmann, C.F., Behrens, T.E., Johansen-Berg, H., Bannister, P.R., De Luca, M., Drobnjak, I., Flitney, D.E. *et al.* (2004) Advances in functional and structural MR image analysis and implementation as FSL. *NeuroImage*, **23** **Suppl 1**, S208-219.
- 41 Jiang, M. and Chen, G. (2006) High Ca²⁺-phosphate transfection efficiency in low-density neuronal cultures. *Nat Protoc*, **1**, 695-700.

LEGENDS TO FIGURES

Figure 1.

Analysis of brain weight and volume in *Dym*^{-/-} mutant mice.

(A): Brains from WT (*Dym*^{+/+}) and *Dym* mutant (*Dym*^{-/-}) mice at P30. Dashed lines delimit the rostrocaudal extent of the cerebral cortex (Cx). OB, Olfactory Bulb, Cb, Cerebellum.

(B): Brain weight of P0, P5 and P30 WT (*Dym*^{+/+}), heterozygous (*Dym*^{+/-}) and homozygous mutant (*Dym*^{-/-}) mice. Quantitative data are expressed as means ± SEM for WT (n = 9, 31 and 37 at P0, P5 and P30, respectively), heterozygous (n = 17, 58 and 46 at P0, P5 and P30, respectively) and homozygous mutant mice (n = 18, 18 and 23 at P0, P5 and P30, respectively). Results were compared using one-way ANOVA followed by a post hoc Bonferroni multiple comparison test. (**: p < 0.01, ***: p < 0.001). Brain weight was reduced in all mutant mice from P5 onward.

(C): Brain volumetric MRI from adult *Dym*^{+/+} and *Dym*^{-/-} mice (n = 5). Regions of significant volume reduction in experimental mice compared to controls are shown overlaid in blue/green on the MRI template image. Color indicates estimated p-values as shown by the color bar. P-values are uncorrected for multiple comparisons. Note the local volumetric reductions in the frontal cortex (arrowhead), white matter (asterisks) and inferior structures from *Dym*^{-/-} mice, including brain stem (arrows).

Figure 2.**Brain histomorphometric analysis of adult *Dym*^{-/-} mutant mice.**

(A): Cresyl-violet staining of 16 µm coronal microtome sections of P30 brains from WT and *Dym*^{-/-} mice. The neocortex is highlighted in dark blue, the external capsule and corpus callosum are highlighted in yellow. Dashed lines delimit the dorsoventral axis (DV). AP, anteroposterior axis; ML, mediolateral axis. Representative brain sections in each of the 5 selected rostrocaudal planes (a-e) are shown according to the Franklin/Paxinos Mouse Brain atlas (3rd edition): plane a: anterior section without the corpus callosum (plates 17-19); plane b: anterior section including the corpus callosum (plates 22-23); plane c: medial section with a visible anterior commissure (plates 29-30); plane d: medial section including the hippocampus and dentate gyrus (plates 42-43); plane e: posterior section without the corpus callosum (plates 50-51).

(B): Measurements of brain size of WT (white bars) and *Dym*^{-/-} mice (black bars) along the anteroposterior (AP) and the dorsoventral (DV) axes. Ten to 14 animals per group were used. Results were compared using the Mann-Whitney U test. A two-tailed $p < 0.05$ was considered significant. AP axis and anterior part of DV axis were significantly reduced in *Dym*^{-/-} mice.

(C): Measurements of the surface area of the neocortex (highlighted in blue) from WT (white bars) and *Dym*^{-/-} mice (black bars) at P30. Twenty-four animals per group were used. Results were compared using the Mann-Whitney U test. A two-tailed $p < 0.05$ was considered significant. Note that surface area of the frontal neocortex was significantly reduced.

(D): Measurements of white matter area (highlighted in yellow) composed of the corpus callosum and the external capsule. Ten to 14 animals per group were used. Results were compared using the Mann-Whitney U test. A two-tailed $p < 0.05$ was considered significant. Note that white matter area from *Dym*^{-/-} mice was reduced in all planes.

Figure 3.**Analysis of the expression of myelin basic protein (MBP) in *Dym*^{-/-} mice.**

(A): Double immunofluorescence for Cux1 (red, used as a specific marker for cortical layers II-III) and Ctip2 (green, used as a specific marker for cortical layers IV-VI) and Dapi staining (blue) in the anterior cortex (plane a) from WT and *Dym*^{-/-} mice at P30. Scale bar = 100 μ m. (B): Cortical thickness measurements in layers II-III, IV-VI and I-VI (n = 7). Results were compared using a 2-way ANOVA followed by a post hoc Bonferroni multiple comparison test (***: p<0.001). Note that the significant reduction of frontal cortical thickness in *Dym*^{-/-} mice is associated with a shortening of the deeper layers (C): Determination of cell density in layers II-III and V-VI (n = 12). Results were compared using a 2-way ANOVA followed by a post hoc Bonferroni multiple comparison test. (D): Immunohistochemical analysis of MBP in the corpus callosum of WT and *Dym*^{-/-} mice at P30. (E): Measurement of MPB-positive surface and densitometric quantification of MBP labeling intensity in the corpus callosum of WT and *Dym*^{-/-} mice. Ten to 14 animals per group were used. Results were compared using the Mann-Whitney U test. (*: p < 0.05; **: p < 0.001). MBP-positive surface and intensity are reduced in *Dym*^{-/-} mice (F): Western blot analysis of total hemi-brains at P30 using an anti-MBP antibody and densitometric analysis of MBP protein expression levels. Results were compared using the Mann-Whitney U test. (*: p < 0.05). MBP protein level is reduced in the brain of *Dym*^{-/-} mice.

Figure 4.**Myelination in *Dym*^{-/-} mice.**

(A): Electron micrographs of the corpus callosum from sagittal sections of adult WT and *Dym*^{-/-} mice. Note that the myelin sheath appears thinner, less compact and not properly rolled in *Dym*^{-/-} animals. Scale bars = 1 μ m.

(B): The diameter of myelinated axons was measured from axonal cross-sections. Six animals each from the WT and *Dym*^{-/-} groups were used. For each animal, images were acquired at 3 dorsoventral positions of 3 rostrocaudal levels. The thickness of the myelin sheath was assessed by determining the G-ratio (axon diameter/total fiber diameter). Three hundred measurements of myelinated axons per animal were performed, using ImageJ 1.410 software (NIH) and axons were then pooled by size according to their small (0.2-0.4 μ m), medium (0.4-0.8 μ m) or big diameter (>0.8 μ m). Results were compared using one-way ANOVA followed by a post hoc Bonferroni multiple comparison post-test (***: $p < 0.001$). Both the number of axons and their diameter are similar in WT and *Dym*^{-/-} mice whereas the G-ratio is higher in *Dym*^{-/-} mice than in WT mice.

(C, D): Immunohistochemical analysis and counts of Olig2- and APC-positive cells in the corpus callosum of WT and *Dym*^{-/-} mice at P30. Note that the number of oligodendrocytes is reduced in *Dym*^{-/-} mice. Scale bars = 1 mm (lower magnification) and 50 μ m (higher magnification).

Figure 5.**Morphology of the Golgi apparatus and MBP expression in primary cultures from WT and *Dym*^{-/-} mice.**

(A): Immunocytochemical analysis of the *cis*-Golgi marker GM130 in neurons labeled with NeuN and in oligodendrocytes labeled with the cytoplasmic marker APC. The Golgi apparatus from *Dym*^{-/-} animals is greatly enlarged. Scale bar = 10 μ m.

(B): Increased Golgi area in primary cultured neurons and oligodendrocytes from *Dym*^{-/-} mice when compared to WT mice. Approximately 150 cells were analyzed, using ImageJ 1.410 software (NIH). Results were compared using the Mann-Whitney U test (***: $p < 0.001$).

(C): Immunohistochemical analysis of oligodendrocytes cell death in the corpus callosum at P5 by Terminal deoxynucleotidyl transferase dUTP nick end labeling (TUNEL) and Olig2 staining (upper insets). Note the presence of TUNEL-positive oligodendrocytes in the corpus callosum of *Dym*^{-/-} animals (white arrowheads). Immunocytochemical analysis of the myelin basic protein (MBP) in primary oligodendrocytes labeled with Olig2 (lower insets). *Dym*^{-/-} oligodendrocytes poorly express MBP and display a less branched morphology than the wild-type cells. Scale bar = 10 μ m.

(D): Quantification of oligodendrocytes cell death in the corpus callosum at P5 by TUNEL-positive ($n = 10$, right) and cleaved-caspase 3 ($n = 20$, left) -positive nuclei countings (upper graphs). Cell death is significantly higher in *Dym*^{-/-} animals than in wild type. Results were compared using the Mann-Whitney U test (**: $p < 0.01$, ***: $p < 0.001$). Note the reduced number of oligodendrocytes able to express MBP and the significant reduction of MBP-positive area in primary cultured oligodendrocytes from *Dym*^{-/-} mice when compared to WT mice (lower graphs). Approximately 150 cells were analyzed, using ImageJ 1.410 software (NIH). Results were compared using the Mann-Whitney U test (***: $p < 0.001$).

Figure 6.**Functional analysis of ER-to-Golgi trafficking using the Retention Using Selective Hooks (RUSH) system in primary cultures of cortical neurons from WT and *Dym*^{-/-} mice.**

Retention and release analysis of the Golgi enzyme mannosidase II fused to SBP-GFP (ManII-SBP-GFP) in the absence (non-treated) or presence of biotin (60 and 120 min incubation). In non-treated cultures, ManII-SBP-GFP (green) is sequestered in the ER (co-localized with the ER marker Calnexin (Calx, red)) by the KDEL hook in both WT and *Dym*^{-/-} neurons. Upon biotin addition, ManII-SBP-GFP is released into the Golgi apparatus (co-localized with the Golgi marker GM130 (pink)) where it is found in all transfected neurons from WT cultures after 120 min. In neurons from *Dym*^{-/-} cultures, the Golgi translocation of ManII-SBP-GFP is strongly delayed. For each condition, an average of 40 neurons was counted and neurons were assigned to three groups depending on whether ManII-SBP-GFP was found in the endoplasmic reticulum (ER), the Golgi apparatus (Golgi), or in both compartments (ER Golgi). Neurons are stained with the neuronal marker MAP2 (red). Results were compared using a 2-way ANOVA followed by a post hoc Bonferroni multiple comparison test (*: $p < 0.05$, **: $p < 0.01$, ***: $p < 0.001$).

Figure 7.**Functional analysis of ER-to-Golgi trafficking using the Retention Using Selective Hooks (RUSH) system in primary fibroblasts from a control and two DMC patients.**

Retention and release analysis of the Golgi enzyme Mannosidase II fused to SBP-GFP (ManII-SBP-GFP) in the absence (non-treated) or presence of biotin (60 and 120 min incubation). In non-treated cultures, ManII-SBP-GFP is sequestered in the ER by the KDEL hook as expected in both WT and DMC fibroblasts. Upon biotin addition, ManII-SBP-GFP is released into the Golgi apparatus where it is found in all transfected cells from WT cultures after 120 min. In contrast, in fibroblasts from DMC cultures, the Golgi translocation of ManII-SBP-GFP is strongly delayed. Primary fibroblasts were transfected at passages P8-10. Fibroblasts from DMC Patients 1 and 2 carry distinct homozygous mutations in *DYM* (g.IVS3-1G>A and c.1877delA, respectively). Cells were assigned to three groups depending on whether ManII-SBP-GFP was found in the endoplasmic reticulum (ER), the Golgi apparatus (Golgi), or in both compartments (ER Golgi). For each condition, an average of 100 transfected fibroblasts was counted. Results were compared using a 2-way ANOVA followed by a post hoc Bonferroni multiple comparison test (**: $p < 0.01$, ***: $p < 0.001$).

Figure 8.**Brain MRI in DMC syndrome.**

(A): Axial and sagittal T2-weighted cranial MRI images from two unrelated patients at 2 years of age with DMC carrying the p.Q483X truncating mutation in the *DYM* gene, and an age-matched control individual. Note the strong reduction in the thickness of the corpus callosum in both patients (white arrows), and the relatively thinner brain stem in Patient 2.

(B): Growth chart tracking the head circumference of DMC Patient 1 (girl) and Patient 2 (boy) from birth, compared to age- and sex-matched population means (X curve). Solid lines show the mean head circumference at various ages. Dashed lines show the limits of two standard deviations above and below the mean circumference. Note that head circumference was normal at birth for both patients and that the development of microcephaly became obvious postnatally, after 12 months of age in Patient 1 and after 2 years in Patient 2.

1 **Supplementary Figure 1.**

2
3 **Morphology of the Golgi apparatus in primary fibroblasts from a control and a DMC**
4 **patient and in neurons and oligodendrocytes derived from WT and *Dym*^{-/-} ES cells**
5 **differentiated *in vitro*.**
6
7
8

9
10
11
12 **(A):** Immunocytochemical analysis of Golgi markers GM130 and Giantin in control and DMC
13 fibroblasts from a patient carrying the loss-of-function mutation g.IVS3-1G>A. Note that, as seen
14 in *Dym*^{-/-} neurons, the Golgi apparatus is greatly enlarged in primary fibroblasts from the DMC
15 patient.
16
17
18

19
20
21 **(B):** Immunocytochemical analysis of GM130 in ES-derived neurons (MAP2) and
22 oligodendrocytes (Olig2). Note that, as in primary *Dym*^{-/-} neurons and oligodendrocytes, the
23 Golgi apparatus appears enlarged and fragmented in ES cell-derived neurons and
24 oligodendrocytes.
25
26
27
28
29
30
31
32
33
34
35
36
37
38
39
40
41
42
43
44
45
46
47
48
49
50
51
52
53
54
55
56
57
58
59
60

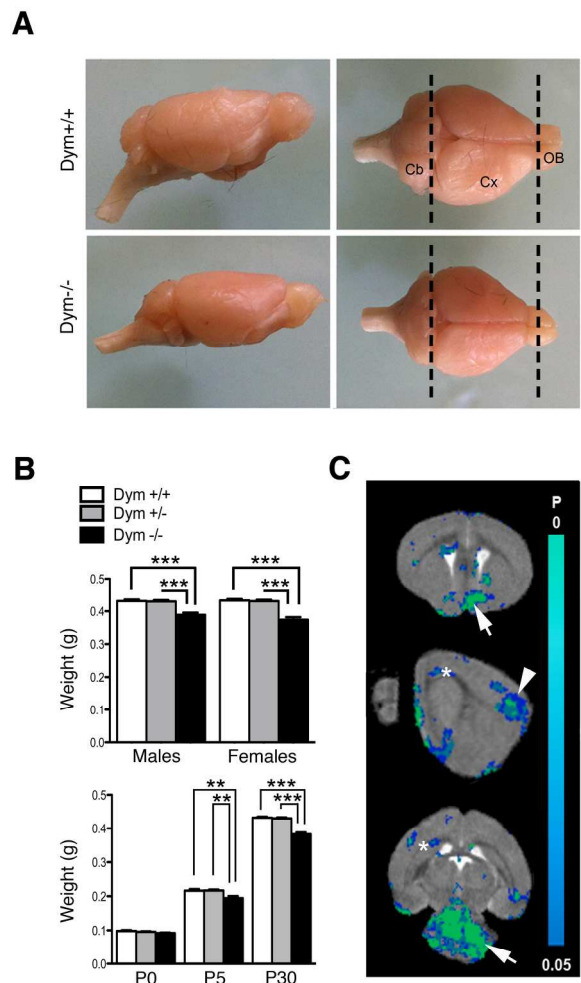
Supplementary Figure 2.**Rescue of defective ER-to-Golgi trafficking using the Retention Using Selective Hooks (RUSH) system in primary cultures re-expressing WT Dymeclin.**

Retention and release analysis of the Golgi enzyme Mannosidase II fused to SBP-mCherry (ManII-SBP-mCh) in the presence of biotin (120 min incubation) and the presence or absence of Dym-GFP.

(A): Primary cultures of cortical neurons from WT and *Dym*^{-/-} mice. Neurons were assigned to three groups depending on whether ManII-SBP-GFP was found in the endoplasmic reticulum (ER), the Golgi apparatus (Golgi), or in both compartments (ER Golgi). For each condition, at least 50 transfected neurons were counted. Results were compared using a 2-way ANOVA followed by a post hoc Bonferroni multiple comparison test. (***: $p < 0.001$). Note that upon Dym-GFP overexpression, ManII-SBP-mCh is localized in the Golgi apparatus of all WT and *Dym*^{-/-} neurons.

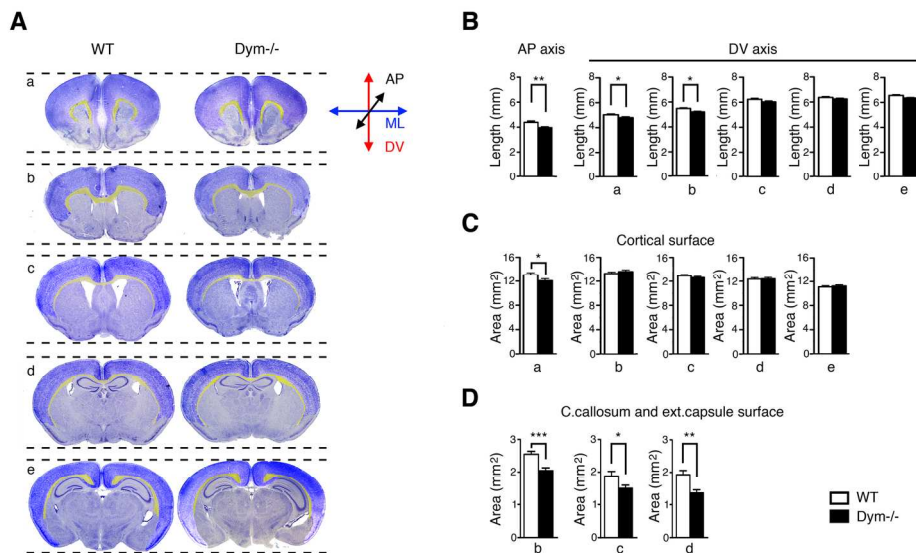
(B): Primary fibroblasts from a healthy control and DMC Patient 1 were transfected at passages P8-10. Cells were assigned to three groups depending on whether ManII-SBP-GFP was found in the endoplasmic reticulum (ER), the Golgi apparatus (Golgi), or in both compartments (ER Golgi). For each condition, at least 70 transfected fibroblasts were counted. Results were compared using a 2-way ANOVA followed by a post hoc Bonferroni multiple comparison test. (***: $p < 0.001$). Note that upon Dym-GFP overexpression, ManII-SBP-mCh is localized in the Golgi apparatus of all control and DMC cells.

1
2
3
4
5
6
7
8
9
10
11
12
13
14
15
16
17
18
19
20
21
22
23
24
25
26
27
28
29
30
31
32
33
34
35
36
37
38
39
40
41
42
43
44
45
46
47
48
49
50
51
52
53
54
55
56
57
58
59
60



Dupuis et al, Figure 1

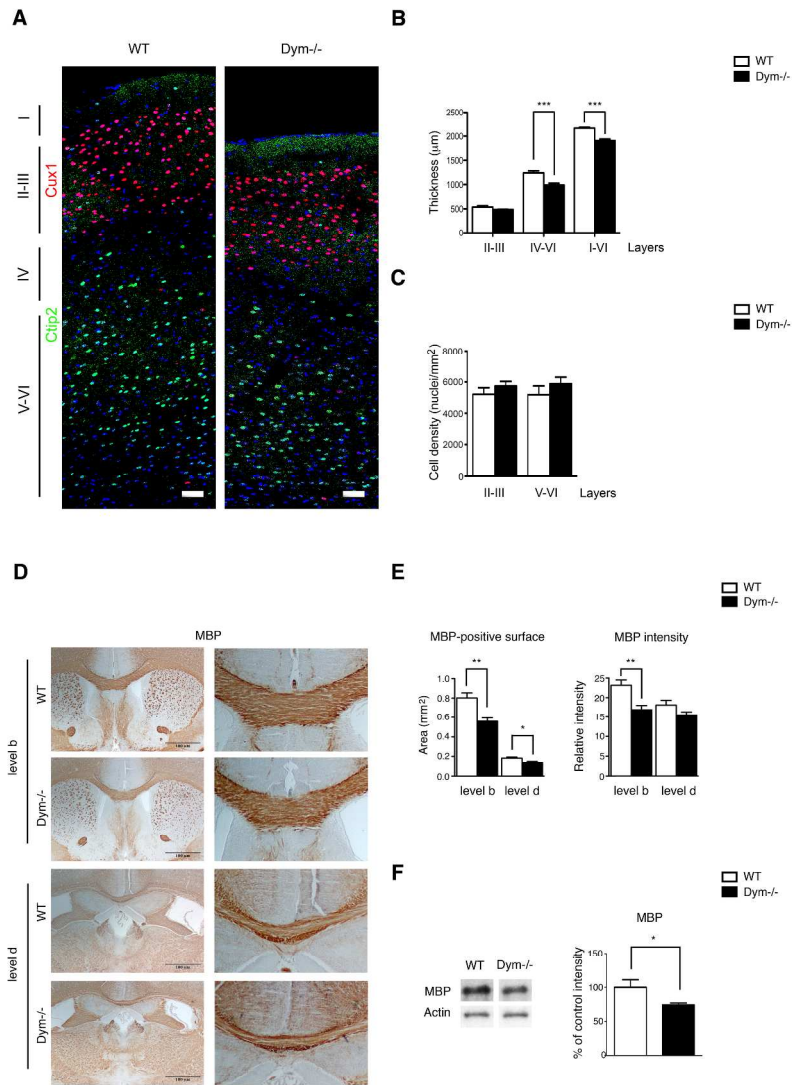
187x262mm (300 x 300 DPI)



Dupuis et al, Figure 2

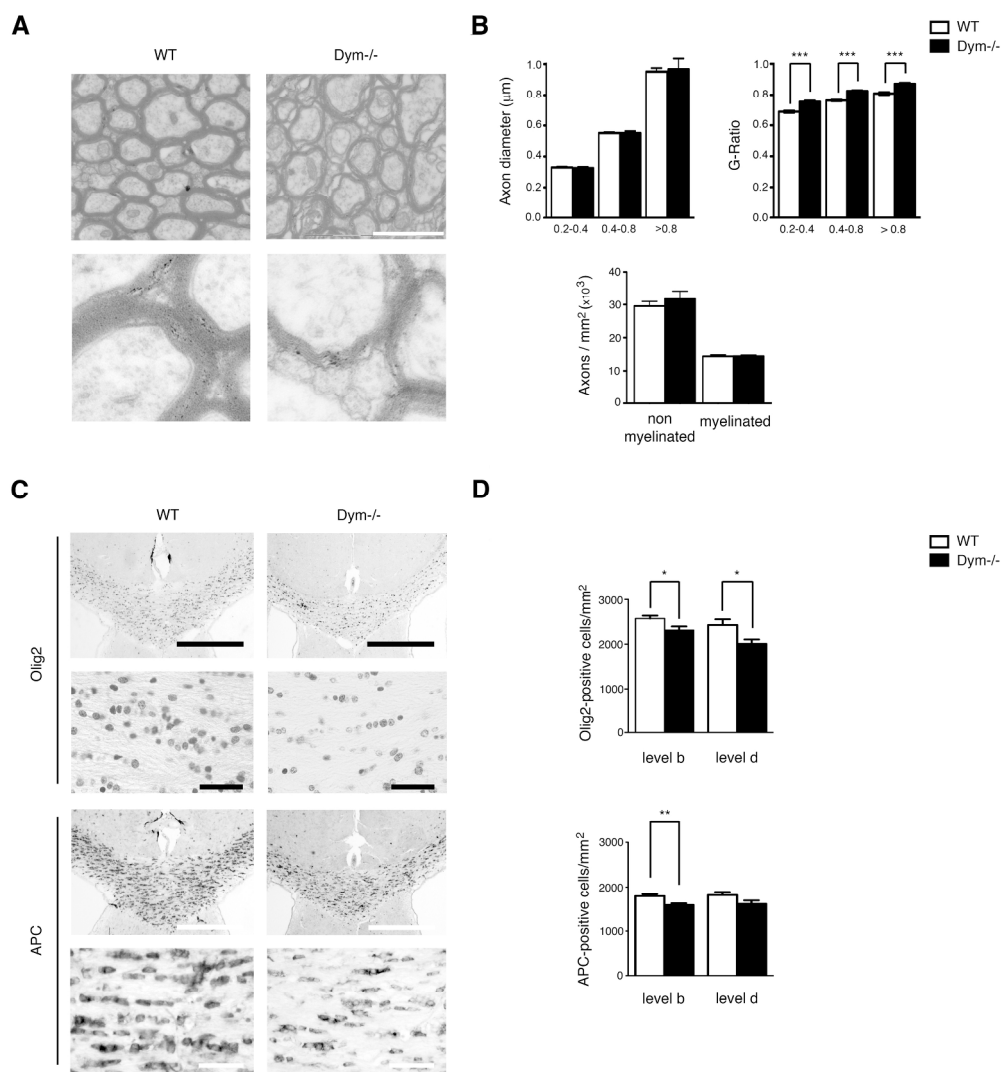
172x157mm (300 x 300 DPI)

1
2
3
4
5
6
7
8
9
10
11
12
13
14
15
16
17
18
19
20
21
22
23
24
25
26
27
28
29
30
31
32
33
34
35
36
37
38
39
40
41
42
43
44
45
46
47
48
49
50
51
52
53
54
55
56
57
58
59
60



Dupuis et al, Figure 3

278x401mm (300 x 300 DPI)

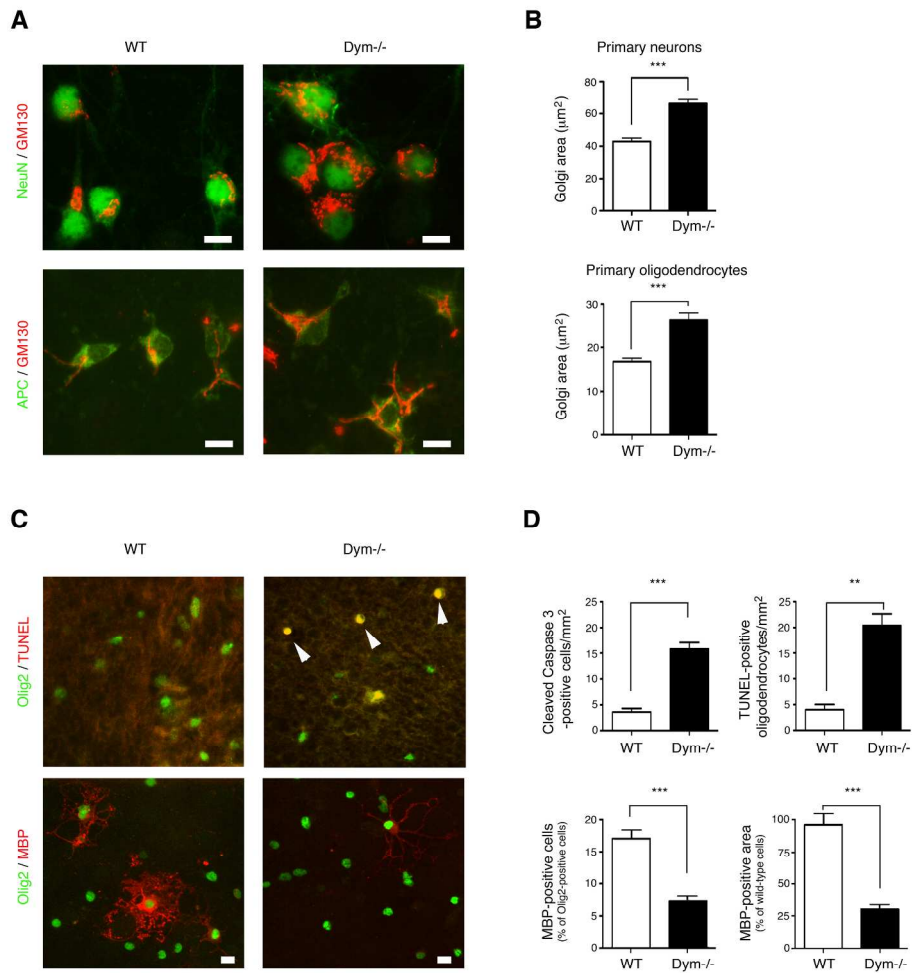


Dupuis et al, Figure 4

229x273mm (300 x 300 DPI)

1
2
3
4
5
6
7
8
9
10
11
12
13
14
15
16
17
18
19
20
21
22
23
24
25
26
27
28
29
30
31
32
33
34
35
36
37
38
39
40
41
42
43
44
45
46
47
48
49
50
51
52
53
54
55
56
57
58
59
60

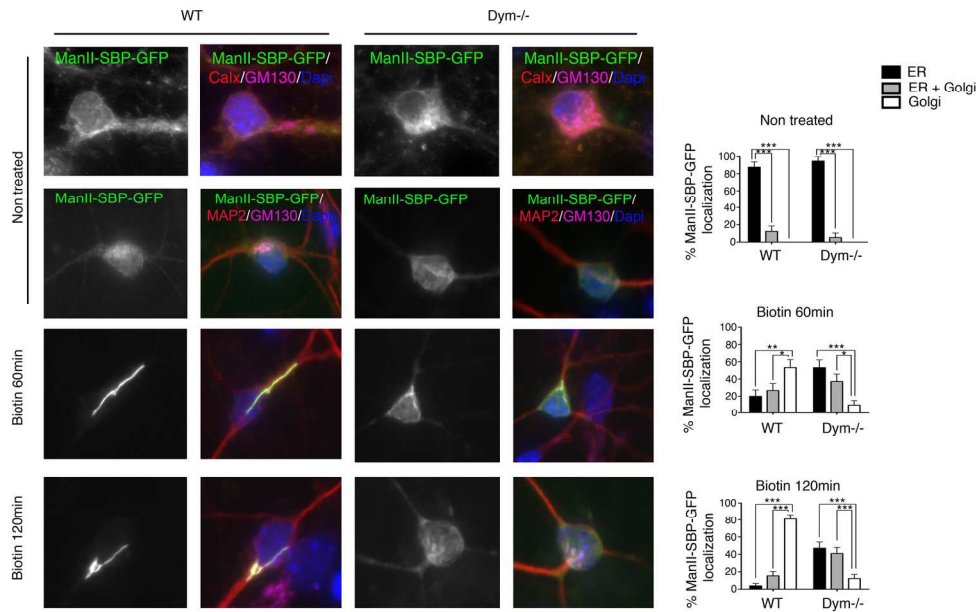
1
2
3
4
5
6
7
8
9
10
11
12
13
14
15
16
17
18
19
20
21
22
23
24
25
26
27
28
29
30
31
32
33
34
35
36
37
38
39
40
41
42
43
44
45
46
47
48
49
50
51
52
53
54
55
56
57
58
59
60



Dupuis et al, Figure 5

236x293mm (300 x 300 DPI)

1
2
3
4
5
6
7
8
9
10
11
12
13
14
15
16
17
18
19
20
21
22
23
24
25
26
27
28
29
30
31
32
33
34
35
36
37
38
39
40
41
42
43
44
45
46
47
48
49
50
51
52
53
54
55
56
57
58
59
60

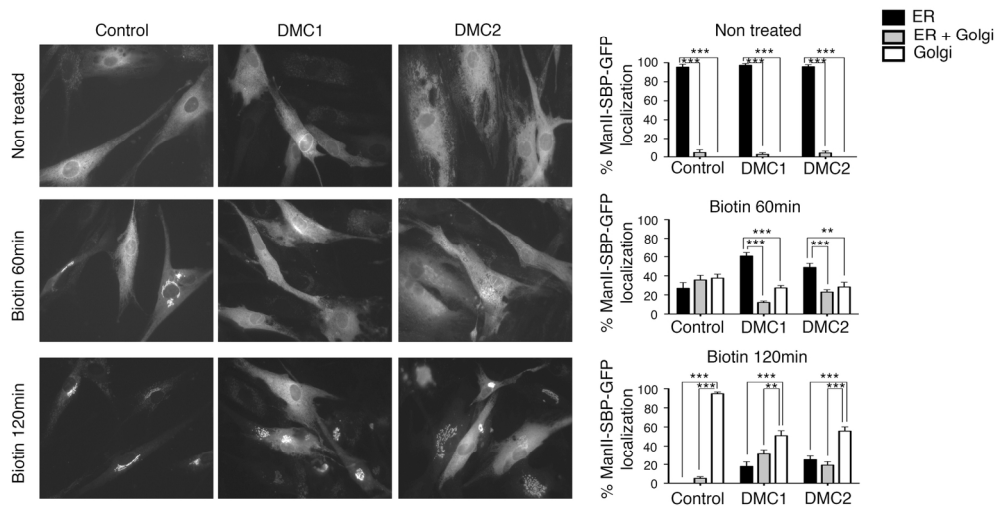


Dupuis et al, Figure 6

171x146mm (300 x 300 DPI)

view

1
2
3
4
5
6
7
8
9
10
11
12
13
14
15
16
17
18
19
20
21
22
23
24
25
26
27
28
29
30
31
32
33
34
35
36
37
38
39
40
41
42
43
44
45
46
47
48
49
50
51
52
53
54
55
56
57
58
59
60

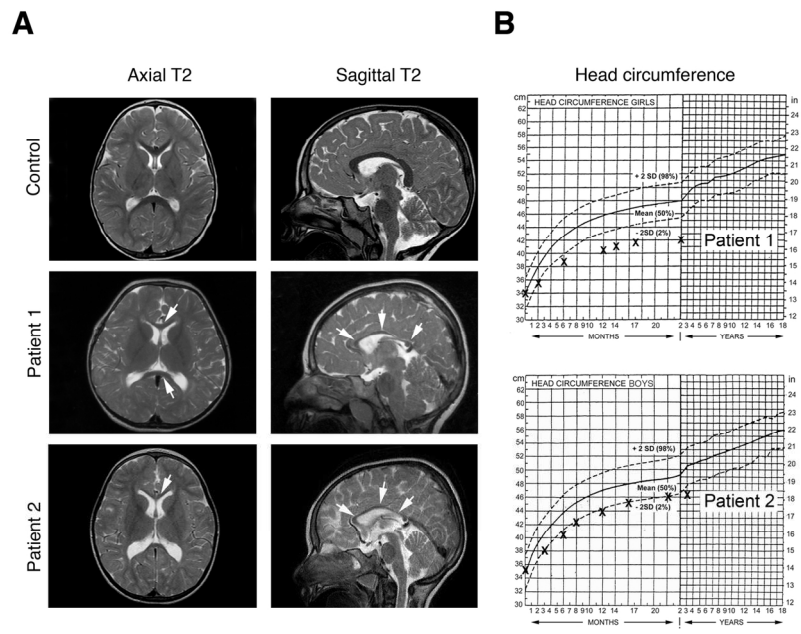


Dupuis et al, Figure 7

157x146mm (300 x 300 DPI)



1
2
3
4
5
6
7
8
9
10
11
12
13
14
15
16
17
18
19
20
21
22
23
24
25
26
27
28
29
30
31
32
33
34
35
36
37
38
39
40
41
42
43
44
45
46
47
48
49
50
51
52
53
54
55
56
57
58
59
60

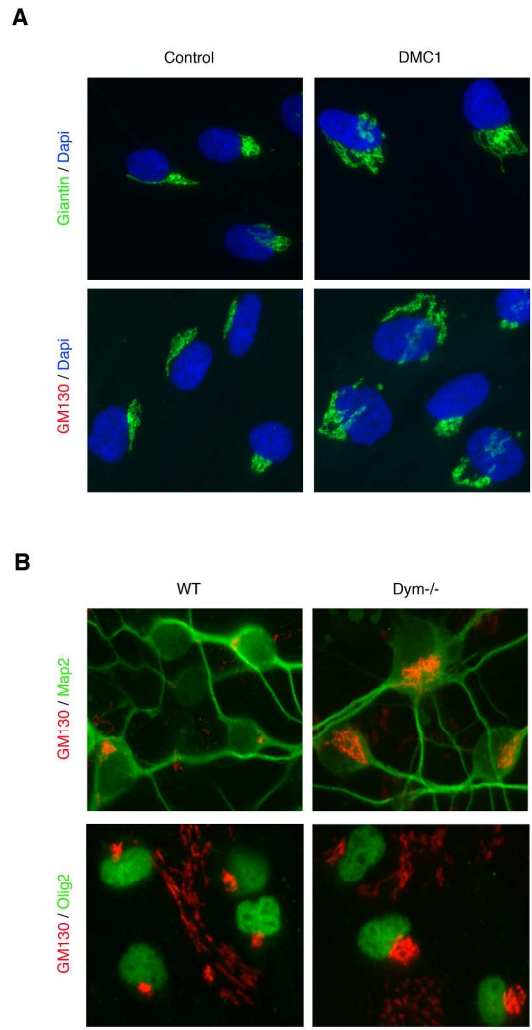


Dupuis et al, Figure 8

153x150mm (300 x 300 DPI)

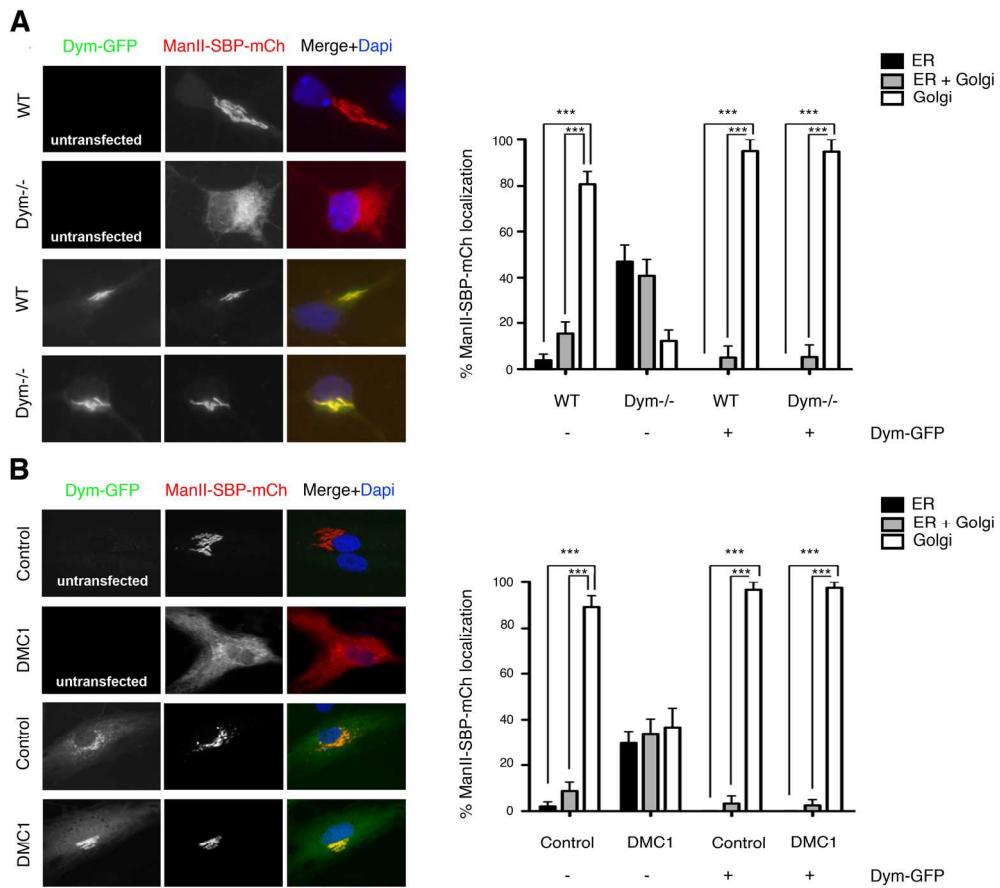


1
2
3
4
5
6
7
8
9
10
11
12
13
14
15
16
17
18
19
20
21
22
23
24
25
26
27
28
29
30
31
32
33
34
35
36
37
38
39
40
41
42
43
44
45
46
47
48
49
50
51
52
53
54
55
56
57
58
59
60



Dupuis et al, Supplementary Figure 1

217x394mm (300 x 300 DPI)



Dupuis et al, Supplementary Figure 2

177x188mm (300 x 300 DPI)

1
2
3
4
5
6
7
8
9
10
11
12
13
14
15
16
17
18
19
20
21
22
23
24
25
26
27
28
29
30
31
32
33
34
35
36
37
38
39
40
41
42
43
44
45
46
47
48
49
50
51
52
53
54
55
56
57
58
59
60